

## Supplemental Data

### Architecture-Dependent Noise

### Discriminates Functionally Analogous

### Differentiation Circuits

Tolga Çağatay, Marc Turcotte, Michael B. Elowitz, Jordi Garcia-Ojalvo, and Gürol M. Süel

#### SUPPLEMENTAL EXPERIMENTAL PROCEDURES

<b>S1. MATHEMATICAL MODELING</b> .....	<b>2</b>
<b>S1.1. The native competence gene regulatory circuit of <i>B. subtilis</i></b> .....	<b>2</b>
S1.1.1 Deterministic description .....	2
S1.1.2 Stochastic description.....	4
<b>S1.2. A synthetic excitable circuit (SynEx)</b> .....	<b>6</b>
S1.2.1 Deterministic description .....	6
S1.2.2 Optimization of the SynEx circuit via phase space analysis.....	8
S1.2.3 Stochastic description.....	9
<b>S1.3. Discrete stochastic simulations of native and SynEx circuits identify the source of variability in competence duration times.</b> .....	<b>10</b>
<b>S1.4. Global parameter analysis</b> .....	<b>12</b>
<b>S1.5. Model of the SynExSlow strain</b> .....	<b>13</b>
<b>S1.6. Transformation efficiency versus DNA concentration</b> .....	<b>14</b>
<b>S2. MATERIALS AND METHODS</b> .....	<b>16</b>
<b>S2.1. Basic strain construction</b> .....	<b>17</b>
<b>S2.2. Promoter definitions</b> .....	<b>17</b>
<b>S2.3. Construction of the SynEx strain</b> .....	<b>17</b>
S2.3.1 Introduction of an IPTG-inducible <i>comS</i> expression cassette into <i>B. subtilis</i> chromosomal DNA.....	18
S2.3.2 Deletion of the <i>B. subtilis</i> endogenous <i>comS</i> gene .....	18
S2.3.3 Introduction of SynEx negative feedback loop via P <sub>comG-Kbox1</sub> - <i>mecA</i> <sup>xp</sup> construct .....	19
<b>S2.4. Optimization of the SynEx circuit</b> .....	<b>19</b>
S2.4.1 IPTG calibration of P <sub>Hyperspank</sub> -ComS, for appropriate competence frequency .....	19
S2.4.2 Tuning the affinity of the P <sub>comG</sub> promoter ( $k_m$ ) .....	20
S2.4.3 Tuning MecA degradation.....	21
<b>S2.5. Construction of the WeakS strain</b> .....	<b>21</b>
<b>S2.6. Construction of the HighS strain</b> .....	<b>21</b>
<b>S2.7. Construction of the SynExSlow strain</b> .....	<b>23</b>
<b>S2.8. Strain Statistics</b> .....	<b>24</b>
<b>S2.9. Transformation of <i>B. subtilis</i> strains</b> .....	<b>24</b>
<b>S2.10. Imaging and growth conditions</b> .....	<b>25</b>
S2.10.1 Preparation for microscopy .....	26
S2.10.2 Image analysis .....	26
<b>Supplemental References</b> .....	<b>28</b>

## S1. MATHEMATICAL MODELING

We aim to compare the noise response of two different genetic circuit architectures that exhibit an analogous dynamical function. Specifically, we concentrate on the phenomenon of transient differentiation, which relies on a temporary activation of gene expression that can arise from *excitable* dynamics. In general terms, a system is said to be excitable when it responds to small perturbations of a stable steady state with large transient excursions away from that state, before relaxing back to it. In gene regulatory systems, such a mechanism leads to transient pulses of protein expression, well above its basal activity. These pulses may be triggered stochastically, while the excursions into, and out of, the alternative cellular state have a relatively well-defined shape and duration. The two circuits presented below exhibit this behavior. In what follows, we describe the dynamics of the two circuits with both deterministic and stochastic approaches.

### S1.1. The native competence gene regulatory circuit of *B. subtilis*

Earlier research (Süel et al., 2006) has shown that the stress-driven competence for DNA uptake in *B. subtilis* is regulated by an excitable gene regulatory circuit. This circuit, named *native* in what follows, is shown in Fig. 1a (main text). It is composed of the master regulator of competence ComK, the stress monitoring protein ComS, and the protease adaptor protein MecA. ComK is continuously being expressed at low levels and degraded by MecA via the ClpP-ClpC protease system. Additionally, ComK is known to activate transcription of its own gene, providing a positive feedback loop that could in principle lead to a bistable response (Maamar and Dubnau, 2005; Smits et al., 2005). Switching from the low-ComK to the high-ComK state occurs when ComS levels become high enough (which happens in the presence of stress), since ComS competes with ComK for binding to MecA. This decreases the degradation rate of ComK, and allows the cell to jump to the high-ComK branch. Inhibition of ComS by ComK, however, destabilizes the competent state in this putative bistable switch, leading to excitable dynamics.

#### S1.1.1 Deterministic description

Assuming that the protein levels can be represented as continuous variables, the behavior of the native circuit is described by the following system of two coupled differential equations (Süel et al., 2006)

$$\begin{aligned}\frac{dK}{dt} &= \alpha_k + \frac{\beta_k K^n}{k_k^n + K^n} - \frac{\delta_k K}{1 + K/\Gamma_k + S/\Gamma_s} - \lambda_k K \\ \frac{dS}{dt} &= \alpha_s + \frac{\beta_s}{1 + (K/k_s)^p} - \frac{\delta_s S}{1 + K/\Gamma_k + S/\Gamma_s} - \lambda_s S\end{aligned}\tag{1}$$

where  $K$  and  $S$  represent the concentration of ComK and ComS, respectively. The role of MecA is represented by the  $\delta_k$  and  $\delta_s$  terms, which correspond to the competitive enzymatic degradation of ComK and ComS (the total amount of MecA is assumed to be constant). The model also includes generation terms representing both basal and regulated expression, and linear degradation due to dilution.

The model parameters can be adjusted to agree with a number of experimental observations, including the very existence and duration of the competence events (Süel et al., 2006), and a remarkable robustness of

the system, which maintains excitability for an exceptionally wide range of stress levels (Süel et al., 2007). For those parameters, given in Table S1, the dynamics of the deterministic native model is represented in the phase portrait shown in Figure S1. In the figure, the red and green lines denote the *nullclines* of  $K$  and  $S$ , respectively, where the corresponding time derivative is zero. These curves organize the phase space, dividing it into regions where the growth/decay tendencies of  $K$  and  $S$ , given by the signs of their derivatives, are well defined (see arrows in Figure S1).

Parameter	Value	Parameter	Value	Parameter	Value
$\alpha_k$	0.00875 molec/s	$\delta_k, \delta_s$	0.001 s <sup>-1</sup>	$k_k$	5000 molec
$\alpha_s$	0.0004 molec/s	$\lambda_k, \lambda_s$	10 <sup>-4</sup> s <sup>-1</sup>	$k_s$	833 molec
$\beta_k$	7.5 molec/s	$\Gamma_k$	25000 molec	$n$	2
$\beta_s$	0.06 molec/s	$\Gamma_s$	20 molec	$p$	5

**Table S1.** Parameters used in the deterministic equations of the native model. The values of the parameters are given in molecule numbers. Assuming a cell volume of 1.66  $\mu\text{m}^3$ , a concentration of one molecule per cell corresponds to 1nM (see Sec. S1.1.2 below).

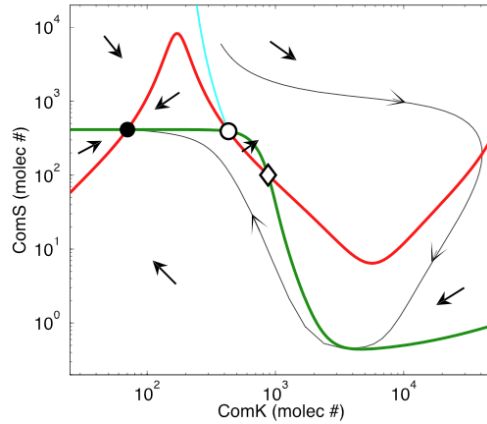


**Figure S1.** Phase-plane portrait of the native circuit. The red (green) line represents the nullcline of ComK (ComS). The cyan line is the excitability threshold. The gray line is a typical excitable trajectory. The arrows show the tendencies of ComK and ComS in each region of phase space delimited by the nullclines.

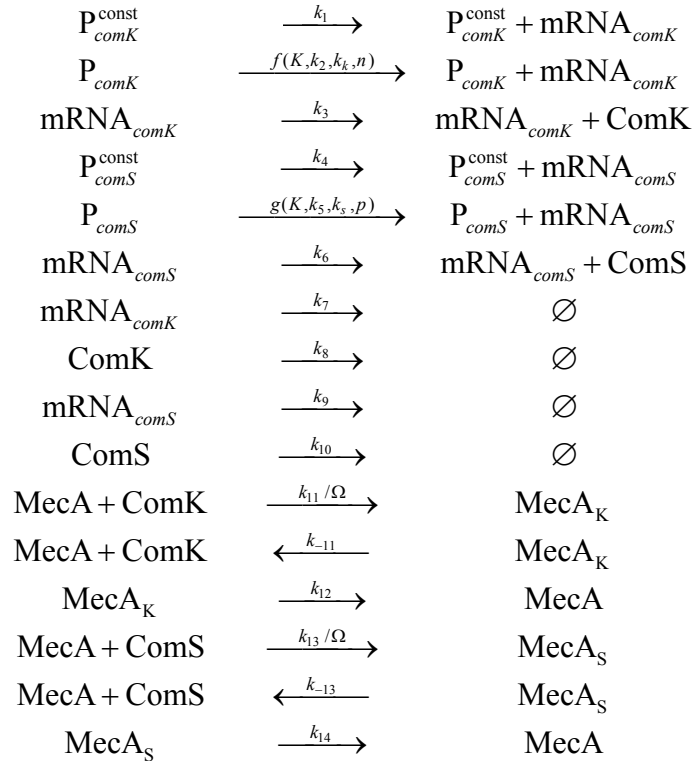
The points where the nullclines cross correspond to fixed points of the system. In our case there are three fixed points, only one of which (represented by a filled circle) is stable; a second one (empty circle) is a saddle point, whereas the third one (empty diamond) is an unstable spiral point. The cyan line is a separatrix<sup>1</sup>, to the right of which the system behaves in an excitable manner: an example of excitable trajectory, triggered by a perturbation that takes the system beyond the separatrix, is represented by the gray line. Note that, once the system is placed to the right of the cyan line, it is forced by the slope field

<sup>1</sup> Mathematically, the separatrix corresponds to the stable manifold of the saddle point.

(i.e. the sign of the derivatives of  $K$  and  $S$  at that point), to move further to the right, into the competence region, and then down and to the left, back to the vegetative state. Thus once triggered (which can happen by means of a stochastic perturbation), the trajectory is fully determined: the system is forced to follow a pre-defined path around phase space on its way back to the stable fixed point.

### S1.1.2 Stochastic description

The continuous description outlined above allows us to establish the potential dynamical outcomes of the native circuit, under given conditions and parameters. However, the proteins involved in the circuit, in particular ComK in the vegetative state, are present in small numbers in the cell, and thus stochastic effects become non-negligible in the dynamics of the genetic module. This stochasticity is also functionally relevant, since it provides the source of perturbations that trigger excitable differentiation events, as has been shown experimentally (Süel et al., 2007). Therefore, a stochastic description of the circuit dynamics is necessary. To that end, the reactions that take place between ComK and ComS must be accounted for explicitly. These reactions include transcription of ComK and ComS, linear degradation of the two proteins and the corresponding mRNA molecules, and their competitive degradation of the two proteins by MecA (Süel et al., 2007):



Here  $P_{gene}$  denotes the promoter of the corresponding gene, constitutive or regulated, and  $MecA_K$  and  $MecA_S$  represent the complex of MecA bound to ComK and ComS, respectively. The transcription of ComK and ComS from their corresponding regulated promoters is given by the following Hill functions:

$$f(K, k_2, k_k, n) = \frac{k_2 K^n}{k_k^n + K^n}, \quad g(K, k_5, k_s, p) = \frac{k_5}{1 + (K/k_s)^p}$$

The forward rates of the bimolecular reactions are scaled by a factor  $\Omega$  that depends on the cell volume  $V$  according to the expression  $\Omega = VA$ , where  $A$  is Avogadro's number (Gillespie, 1977). For  $V = 1.66 \mu\text{m}^3$ , the resulting volume factor is  $\Omega = 1 \text{ molec/nM}$ .

Applying standard reaction kinetics rules, one can write down the rate equations underlying the set of reactions given above. The equations can then be further simplified by adiabatically eliminating the dynamics of the mRNAs, and of the competitive degradation processes, all of which are substantially faster than all other biochemical reactions in the circuit. The resulting set of equations is formally identical to Eqs. (1), and the comparison between the two allows one to relate the deterministic and stochastic parameters (Süel et al., 2007). A set of reaction rates that is compatible with the deterministic parameters of Table S1, for which the system is excitable, is given in Table S2.

$k_1$	$0.00022 \text{ s}^{-1}$	$k_7$	$0.005 \text{ s}^{-1}$	$k_{12}$	$0.05 \text{ s}^{-1}$
$k_2$	$0.19 \text{ s}^{-1}$	$k_8$	$10^{-4} \text{ s}^{-1}$	$k_{13}$	$4.5 \cdot 10^{-6} \text{ molec}^{-1} \text{ s}^{-1}$
$k_3$	$0.2 \text{ s}^{-1}$	$k_9$	$0.005 \text{ s}^{-1}$	$k_{-13}$	$5 \cdot 10^{-5} \text{ s}^{-1}$
$k_4$	0	$k_{10}$	$10^{-4} \text{ s}^{-1}$	$k_{14}$	$4 \cdot 10^{-5} \text{ s}^{-1}$
$k_5$	$0.0015 \text{ s}^{-1}$	$k_{11}$	$2.0 \cdot 10^{-6} \text{ molec}^{-1} \text{ s}^{-1}$	$M_T$	500 molec
$k_6$	$0.2 \text{ s}^{-1}$	$k_{-11}$	$5 \cdot 10^{-4} \text{ s}^{-1}$		

**Table S2.** Reaction rates of the stochastic native model.

A standard Monte Carlo simulation of the set of reactions given above, with the parameters given in Table S2 and using the First Reaction method developed by Gillespie (Gillespie, 1977) produces excitable stochastic trajectories that fit well with the deterministic picture provided by the nullclines of the differential equation model, as shown in Figure S2.

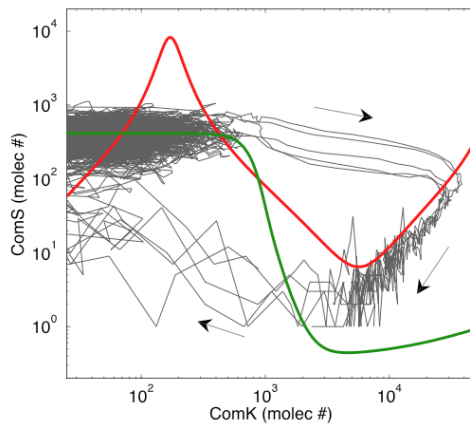


**Figure S2.** Stochastic trajectories of the native circuit. The gray lines represents the trajectories generated by the Gillespie algorithm, and the arrows their direction.

## S1.2. A synthetic excitable circuit (SynEx)

In the native circuit described above, ComK is both an activator of its own expression and an inhibitor of the expression of ComS. But excitability in other natural systems, such as neurons, usually relies on the interaction between a pure activator and a pure inhibitor. We have designed a synthetic gene regulatory circuit, named SynEx in what follows and shown in **Fig. 1B** (main text), that includes two such elements, making partial use of the natural native circuit. In the SynEx strain, ComK activates transcription of both its own *comK* gene and the *mecA* gene. To that end, a copy of the latter gene is placed under the control of the  $P_{comG}$  promoter, which is activated by ComK in an exclusive way. The protein MecA acts as the inhibitory element in the synthetic excitable circuit, since it binds to and degrades ComK via the ClpP-ClpC protease system.

### S1.2.1 Deterministic description

The following set of differential equations describe the biochemical interactions described above:

$$\begin{aligned}\frac{dK}{dt} &= \alpha_k + \frac{\beta_k K^n}{k_k^n + K^n} - \delta KM - \lambda_k K \\ \frac{dM}{dt} &= \alpha_m + \frac{\beta_m K^p}{k_m^p + K^p} - \lambda_m M\end{aligned}\tag{2}$$

Here  $K$  denotes the concentration of ComK and  $M$  the concentration of MecA. The constant production terms given by  $\alpha_k$  and  $\alpha_m$  represent basal expression from the  $P_{comK}$  and  $P_{comG}$  promoters, respectively, while  $\beta_k$  and  $\beta_m$  measure the maximum rate of regulated expression from these two promoters. Half-maximal activation of these promoters occurs at ComK concentrations denoted by  $k_k$  and  $k_m$ , respectively. The third term on the right-hand side of the ComK equation corresponds to the degradation of ComK by MecA. Linear degradation of the two proteins is measured by the relaxation rates  $\lambda_k$  and  $\lambda_m$ .

Equations (2) can be obtained from the kinetic equations corresponding to the biochemical reactions underlying the SynEx circuit (see below), after an adiabatic elimination of the mRNA dynamics, and assuming that MecA degrades ComK enzymatically (no MecA is assumed to be consumed in the process) and far from saturation (i.e. the corresponding degradation term in the  $K$  equation is linear in  $K$ ).

Since the SynEx circuit shares the ComK-mediated positive feedback loop with the natural native circuit, some of its parameters can be constrained to a certain extent by experimental observations of that system (Süel et al., 2007). In particular, we use the same values of the ComK production and linear degradation rates that are used in the native circuit (see Table S1). On the other hand, the enzymatic degradation of that protein is simplified, as mentioned above, by assuming that MecA is not saturated.

A list of parameter values used in this paper for model (2) is given in Table S3. Note that, with respect to the reference values of the natural competence circuit, the basal expression of MecA is assumed to be around one order of magnitude larger than that of ComK, its linear degradation rate is assumed equal, and the cooperativity coefficient of the  $P_{comG}$  promoter activation (given by the Hill exponent  $p$ ) is assumed to

be the same than that of  $P_{comK}$  (given by  $n$ ), since both promoters are activated by ComK dimers in a presumably similar way.

For the parameters given in Table S3, the circuit operates in an excitable regime, as shown in the left panel of Figure S3. The figure shows, in the phase space formed by  $K$  and  $M$ , the nullclines of these two dynamical variables. As in the case of the native model, the points where the nullclines cross define the fixed points of the system.

Parameter	Value	Parameter	Value	Parameter	Value
$\alpha_k$	0.00875 molec/s	$\beta_m$	2.5 molec/s	$k_k$	5000 molec
$\alpha_m$	0.075 molec/s	$\delta$	$4 \cdot 10^{-8}$ molec $^{-1}$ s $^{-1}$	$k_m$	2500 molec
$\beta_k$	7.5 molec/s	$\lambda_k, \lambda_m$	$10^{-4}$ s $^{-1}$	$n, p$	2

**Table S3.** Parameters used in the deterministic equations of the SynEx model. The values of the parameters are given in molecule numbers. Assuming a cell volume of  $1.66 \mu\text{m}^3$ , a concentration of one molecule per cell corresponds to  $1\text{nM}$  (see Sec. S1.1.2 above).

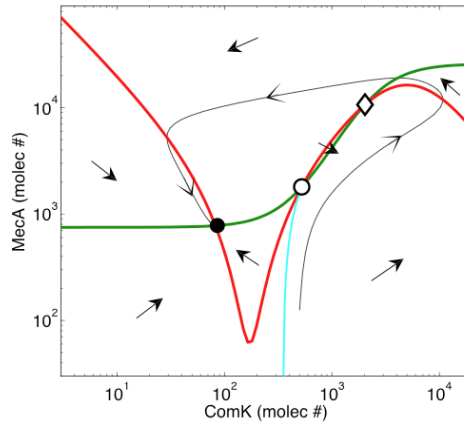


**Figure S3.** Phase-plane portrait of the SynEx circuit. The red (green) line represents the nullcline of ComK (MecA). The cyan line is the excitability threshold. The gray line is a typical excitable trajectory. The arrows show the tendencies of ComK and MecA in each region of phase space delimited by the nullclines.

For the parameters given in Table S3, the SynEx circuit exhibits three fixed points, denoted by symbols in the left panel of Figure S3. Only the low-ComK fixed point happens to be stable, corresponding to the vegetative state. As in the native module, the other two fixed points are unstable, the one at high ComK being an unstable spiral (empty diamond), and the intermediate one being a saddle point (empty circle). The stable manifold of the saddle point (cyan line in left panel of Figure S3) corresponds to the excitability threshold. The figure shows a typical excitable trajectory of the system (gray line). Note that, in contrast to the native system, the vegetative state exhibits a low level of *both* circuit proteins, ComK and MecA, while the competence region corresponds to an area where *both* ComK and MecA are high.

### S1.2.2 Optimization of the SynEx circuit via phase space analysis

Excitable dynamics in the SynEx circuit are only possible for a range of parameters. If for example, the wild-type  $P_{comG}$  promoter, which expresses MecA in the SynEx circuit, has a high affinity for its activator protein, ComK, excitable dynamics are not possible. This situation is shown in the left panel of Figure S4, which depicts as a dashed green line the resulting MecA nullcline when the Michaelis constant of the  $P_{comG}$  promoter (which measures the inverse of the affinity of that promoter for ComK) is assumed to be low (10-fold lower than the corresponding parameter given in Table S1). In that case, there is only a single crossing point between the ComK and MecA nullclines, which corresponds to a single steady state (vegetative growth) whose stability is too large for excitable excursions to occur: the system is not excitable for such low values of  $k_m$ . A possible way of allowing for excitable behavior is by lowering the affinity of the  $P_{comG}$  promoter for ComK. Indeed, when  $k_m$  is increased we recover the situation described in the previous Section, with two additional unstable fixed points in the system that force the cell to follow a large excitable trajectory when pushed beyond the excitability threshold (see again Figure S3). Consistent with this mathematical prediction, a point mutation was introduced experimentally in the  $P_{comG}$  promoter expressing MecA, which indeed led to excitable behavior in SynEx cells (See also Suppl. Section S2.4.2).

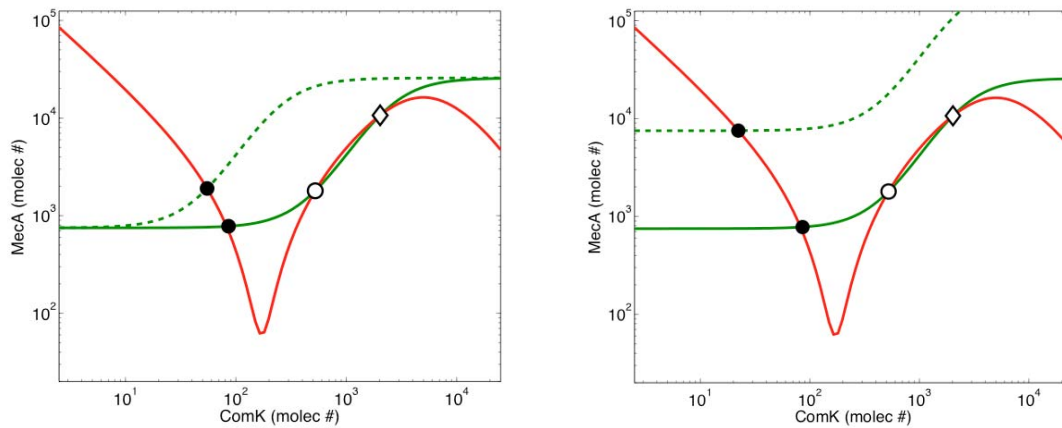
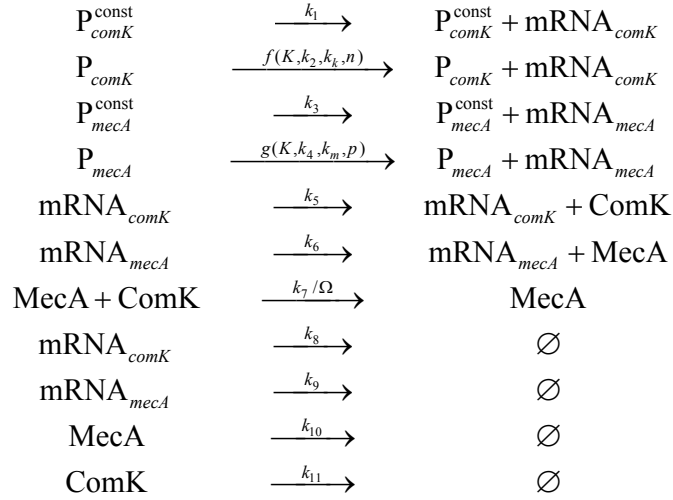


**Figure S4.** Left: effect of decreasing the affinity of the  $P_{comG}$  promoter, as measured by  $k_m$ , from its wild-type value (dashed green line) to a mutated version (solid green line), as done experimentally (see main text). Right: effect of increasing the degradation rate of MecA,  $\lambda_m$ , from its wild-type value (dashed green line) by one order of magnitude (solid green line).

In addition to lowering the strength of  $P_{comG}$ , a second experimental modification was made to the SynEx circuit in order to optimize the excitable behavior of the system. Specifically, decreasing MecA stability (which can be accomplished experimentally by adding a degradation tag to the *mecA* gene that is expressed from the  $P_{comG}$  promoter), can favor excitable dynamics (See also Suppl. Section S2.4.3). The effect of having a small degradation for MecA, as predicted by the theoretical model described above, can be seen in the right panel of Figure S4. The solid green line represents the MecA nullcline for the base parameters given in Table S3, while the dashed green line corresponds to that same nullcline when the degradation rate of MecA is reduced by an order of magnitude, which is closer to the natural degradation level.

### S1.2.3 Stochastic description

The reactions describing the SynEx circuit are:



Just as for the native circuit, ComK promotes its own transcription. Here, however, MecA transcription is placed under ComK control via the  $P_{comG}$  promoter. The corresponding regulatory Hill functions are given by:

$$f(K, k_2, k_k, n) = \frac{k_2 K^n}{k_k^n + K^n}, \quad g(K, k_4, k_m, p) = \frac{k_4 K^p}{k_m^p + K^p}$$

The degradation of ComK via the ClpP-ClpC adaptor protein MecA is simulated by a 2<sup>nd</sup> order binding reaction followed by enzymatic degradation. Other degradation reactions are simple 1<sup>st</sup> order reactions. The simulation was done using Gillespie's direct method (Gillespie, 1976). Resulting dynamics are such that both high MecA and ComK are not favored because high levels of MecA degrade ComK at an increased rate. Thus the system is more likely to be in low MecA and ComK.

To guide our investigations of stochastic regimes, we derived the correspondence between the stochastic differential equation set and the corresponding deterministic equations (2) by making an adiabatic approximation of the promoter dynamics. The set of SynEx stochastic parameters that result in a functional equivalent to the native circuit are given in Table S4.

These parameters lead to excitable dynamics in the SynEx. Figure S5 shows a few typical trajectories in this case. The trajectories orbit in the clockwise direction (as indicated by the arrows), opposite to the native circuit. This happens because of the opposite correlation in concentrations of the negative feedback loop components in the two circuits: while in the native circuit ComK represses ComS, in the SynEx circuit ComK activates MecA.

Parameter	Value	Parameter	Value	Parameter	Value
$k_1$	$0.00022 \text{ s}^{-1}$	$k_6$	$0.2 \text{ s}^{-1}$	$k_{11}$	$0.0001 \text{ s}^{-1}$
$k_2$	$0.19 \text{ s}^{-1}$	$k_7$	$4 \cdot 10^{-8} \text{ molec}^{-1} \text{ s}^{-1}$	$k_k$	5000 molec
$k_3$	$0.0019 \text{ s}^{-1}$	$k_8$	$0.005 \text{ s}^{-1}$	$k_m$	2500 molec
$k_4$	$0.0625 \text{ s}^{-1}$	$k_9$	$0.005 \text{ s}^{-1}$	$n, p$	2
$k_5$	$0.2 \text{ s}^{-1}$	$k_{10}$	$0.0001 \text{ s}^{-1}$		

**Table S4.** Parameters used in the deterministic equations of the SynEx model. The values of the parameters are given in molecule numbers. Again, assuming a cell volume of  $1.66 \mu\text{m}^3$ , a concentration of one molecule per cell corresponds to  $1\text{nM}$  (see Sec. S1.2 above).

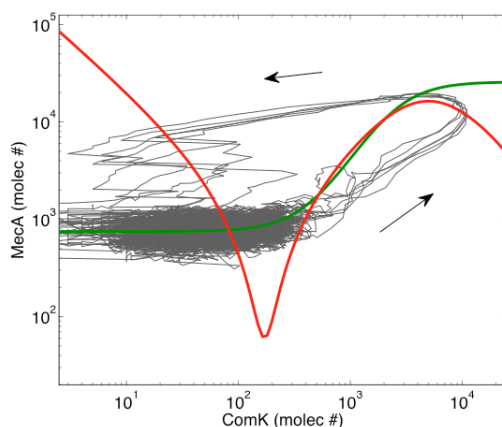


**Figure S5.** Stochastic trajectories of the SynEx circuit. The gray lines represent the trajectories generated by the Gillespie algorithm, and the arrows indicate their direction.

### S1.3. Discrete stochastic simulations of native and SynEx circuits identify the source of variability in competence duration times.

Duration of competence episodes in the native and SynEx circuits are determined by ComS and MecA concentrations respectively. Therefore, we took advantage of variation inherent in discrete stochastic simulations and clustered native and SynEx competence time traces according to their noise in ComS or MecA. For each ComS and MecA noise cluster, we then determined the noise in competence duration times. Higher amplitudes of stochastic fluctuations in ComS during competence increased variability of native competence duration times (Figure S6). In contrast, noise in MecA and competence duration times were relatively smaller in SynEx simulations (Figure S6). Discrete stochastic simulations thus provided an intuitive explanation for the divergence of noise amplitudes observed in competence duration times between the two circuits, based simply on the opposite correlation in molecule numbers of ComS and MecA during competence.

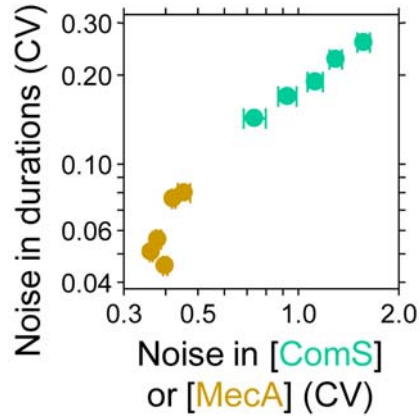


**Figure S6.** Doubly logarithmic plot depicting noise in competence duration times versus the coefficient of variation (noise) in ComS or MecA concentrations during competence. Data points and error bars represent mean and S.E.M., respectively, from analysis of over 150 ComS and MecA time traces each, obtained from discrete stochastic simulations of the native and SynEx circuits. Note the difference in noise amplitudes of ComS and MecA, as well as the corresponding variation in noise of competence duration times for native and SynEx circuits respectively.

We next implemented *in silico* a way to vary the noise in ComS and MecA in a controlled way at the circuit level. The method consists on scaling the strengths of the  $P_{comS}$  and  $P_{mecA}$  promoters, while compensating for these perturbations by varying the corresponding efficiencies of ComS and MecA at activating and inhibiting, respectively, ComK. This procedure can be considered the circuit-level analogy of the method proposed by van Oudenaarden and co-workers to control noise in the expression of a single gene by varying independently the transcription and translation rates (Ozbudak et al., 2002). In our case, since the native strain is more noisy (in terms of competence durations) than the SynEx circuit, we bring the noise in ComS down in the native circuit by scaling up the strength of the  $P_{comS}$  promoter (as measured by the parameters  $\alpha_s$  and  $\beta_s$ ) by a certain factor  $K$ , while scaling down by the same factor the affinity of ComS for the ComK degradation machinery (as measured by the parameter  $1/\Gamma_s$ ). Concurrently, we bring the noise in MecA up in the SynEx circuit by reducing the strength of the  $P_{mecA}$  promoter (as measured by the parameters  $\alpha_m$  and  $\beta_m$ ) by the factor  $K$ , while increasing the rate of binding of MecA and ComK by the same factor. As a result of these perturbations, noise in durations increases in the SynEx circuit as  $K$  increases, as shown in **Fig. 4C** of the main text (where  $K$  is represented by the color coding), while the native circuit is not much affected. Furthermore, the increase in duration noise in the SynEx circuit is associated with a substantial increase of noise in the amplitudes of the ComK peaks, as shown in **Fig. S7** below. Such large variability in peak amplitudes would lead to an imperfect ability of the SynEx circuit to reach in a consistent way high enough ComK levels to successfully produce the competence phenotype in the cell at every pulse instance, as shown in **Fig. 4C** of the main text. Thus, numerical simulations show that the SynEx circuit cannot increase the noise in competence durations arbitrarily without losing its functionality. The native circuit, on the other hand, is consistently noisy in durations while maintaining a high reliability in pulse amplitudes.

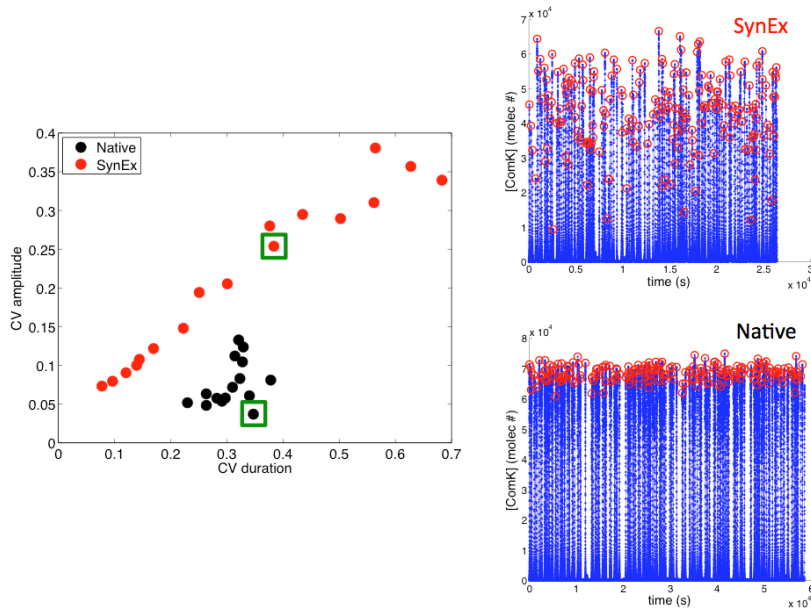


**Figure S7.** Correlation between the duration and amplitude noises in the native and SynEx circuits (left panel). Noise is varied by scaling promoter strengths and affinities by the same noise scaling factor  $K$ , as explained in the text. The time traces on the right panels correspond to selected parameters in the native and SynEx circuits, marked with green squares in the left panel, that have similar levels of noise in the competence durations (0.35 for the native circuit, 0.38 for the SynEx). In particular, the native case corresponds to the wild-type situation. The red circles in the time-trace plots marks the location of the event peaks. A much higher variability in the peak amplitudes (for the same duration noise) is evident in the SynEx.

#### S1.4. Global parameter analysis

In order to establish whether or not the differences in noise behavior between the native and SynEx circuits shown in the preceding Section are generic, we next performed a systematic parameter analysis of the two systems. To that end, we varied *all* the parameters of both circuits in a range of  $\pm 10\%$  around the basal values used to represent the wild-type situation, given in Sections S1.1 and S1.2 above. Of the 70 parameter sets explored in each circuit, 48 sets maintained excitability in the native circuit (69%), while 57 remained excitable in the SynEx case (81%). These figures indicate that excitability is a robust dynamical regime in both systems. Furthermore, the parameter realizations of the two circuits exhibited distinct statistical characteristics when analyzed in terms of competence durations and amplitude of competence events. **Figure S8** plots the mean and CV of the durations, together with the CV of the amplitudes, for all excitable parameter sets in both circuits. The results show that the data points occupy different subspaces in this 3-d state space, which indicates that the two circuit architectures have a characteristic behavior. In particular, only SynEx reaches high CV amplitudes, while only the native circuit can reach arbitrarily high mean durations. These results demonstrate that the architecture determines the noise properties of the circuits in a way that cannot be accomplished by mere parameter variations.

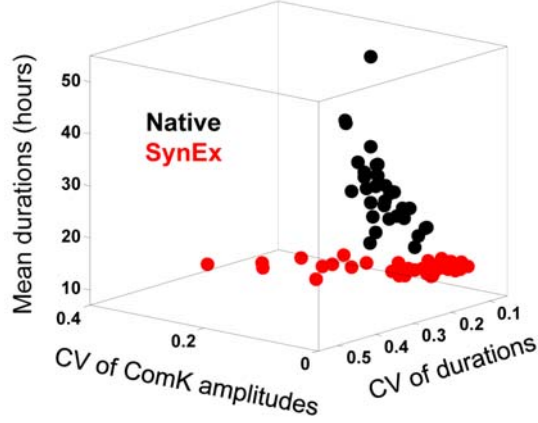


**Figure S8.** Global parameter analysis for native and SynEx circuits. All parameter values of native and SynEx circuits were randomly varied. Plotted are competence properties of random sets of parameter values for each circuit architecture. Note the distinct trends in native and SynEx circuit data points.

### S1.5. Model of the SynExSlow strain

The SynExSlow strain is constructed from the SynEx strain, through the addition of a  $P_{comG}$  promoter that drives the expression of ComS. Consequently, in this strain we can no longer neglect the dynamics of ComS, since its expression is coupled to the amount of ComK in the cell, similarly to what happened in the Native strain. Thus, the model of the SynExSlow strain has three degrees of freedom, for the concentrations of ComK ( $K$ ), MecA ( $M$ ), and ComS ( $S$ ), and is basically a combination of the Native and SynEx models given above:

$$\begin{aligned}\frac{dK}{dt} &= \alpha_k + \frac{\beta_k K^n}{k_k^n + K^n} - \frac{\delta_k MK}{1 + K/\Gamma_k + S/\Gamma_s} - \lambda_k K \\ \frac{dM}{dt} &= \alpha_m + \frac{\beta_m K^p}{k_m^p + K^p} - \lambda_m M \\ \frac{dS}{dt} &= \alpha_s + \frac{\beta_s K^n}{k_s^n + K^n} - \frac{\delta_s MS}{1 + K/\Gamma_k + S/\Gamma_s} - \lambda_s S\end{aligned}$$

Note that in the competitive degradation term of the  $K$  and  $S$  equations we now add explicitly the variable  $M$ , similarly to what we did in the SynEx model (which on the other hand assumed saturation of that reaction in the  $K$  equation). We have also added a term in the  $S$  equation representing the expression of ComS from the  $P_{comG}$  promoter. The values of the parameters used to obtain the deterministic time traces shown in Fig. 5A of the main text are shown in the Table below. Note that the values of the MecA degradation rates  $\delta_k$  and  $\delta_s$  have been redefined by making MecA explicit in the correspond reaction terms. Their values have been chosen to be consistent with the ones assumed in the Native model, considering that in that case the total number of MecA molecules was taken to be 500. The affinity of the

$P_{comG}$  promoter for ComK is assumed to be one order of magnitude higher than the one of the  $P_{comK}$  promoter, while the cooperativity of both reactions is considered the same. Note also that the basal production of ComS, corresponding to expression from the  $P_{hyperspank}$  promoter, is supposed to be of the same order of magnitude as that from the  $P_{comG}$ . All other parameters of this model are consistent with both the Native and SynEx models.

Parameter	Value	Parameter	Value	Parameter	Value
$\alpha_k$	0.00875 molec/s	$\beta_k$	7.5 molec/s	$k_k$	5000 molec
$\alpha_m$	0.075 molec/s	$\beta_m$	2.5 molec/s	$k_m$	2500 molec
$\alpha_s$	0.5 molec/s	$\beta_s$	0.5 molec/s	$k_s$	500 molec
$\delta_k, \delta_s$	$2 \cdot 10^{-6} \text{ molec}^{-1} \text{ s}^{-1}$	$\Gamma_k$	25000 molec	$n$	2
$\lambda_k, \lambda_m, \lambda_s$	$10^{-4} \text{ s}^{-1}$	$\Gamma_s$	20 molec	$p$	2

**Table S5.** Parameters used in the deterministic equations of the SynExSlow strain.

### S1.6. Transformation efficiency *versus* DNA concentration

Here we investigate the effect of variation in competence duration times on the physiological efficiency of competence events. To that end, we evaluate the transformation efficiency of native and SynEx strains under stress conditions and varying concentrations of exogenous DNA. Our hypothesis is that larger variability of competence duration times in the native strain permits successful transformations for a broad range of extracellular DNA concentrations. Consequently, the narrow distribution of competence duration times in the SynEx strain is expected to support successful transformations only for a relatively narrow range of extracellular DNA concentrations. This hypothesis is based on the fact that successful transformation events require that cells encounter DNA molecules while being in the competent state, and thus different distributions of duration times, such as exhibited by our two strains, should lead to divergent sensitivities to DNA concentration. Two characteristic times must therefore be compared: the duration of competence and the diffusion time of DNA in the extracellular medium, which is assumed to be inversely proportional to the DNA concentration,  $\tau_{diff} = k/[DNA]$ . We consider that a transformation is successful when  $\tau_{comp} > \tau_{diff}$ . Therefore, given the experimentally determined distribution of competence duration times,  $P(\tau_{comp})$ , which is given in Fig. 3b of the main text for both genetic circuits, the number of successful transformation events for a certain DNA concentration  $d$  is given by the cumulative distribution function

$$H(d) = \int_{k/d}^{\infty} P(x) dx$$

The result of performing this calculation with the experimental data coming from both the native and SynEx circuits is shown in the left plot of

**Figure S6.** In the figure, solid lines correspond to fittings to a sigmoidal function of  $n$ -th order,

$$H(d) = \frac{ad^n}{d_0^n + d^n}$$

For native cells, the order of the sigmoidal function is  $n=4.07\pm 0.26$ , while for the SynEx cells it is approximately doubled,  $n=8.08\pm 0.61$ . In other words, physiological success of competence events in the SynEx strain is more sensitive to changes in concentration of exogenous DNA. Consequently, transformation efficiency in the noisier native strain is more robust to changes in extracellular DNA concentrations. This prediction is in agreement with results from transformation experiments shown in Fig. 5b of the main text. This difference in sensitivities of transformation efficiencies between the native and SynEx strains does not stem from the difference in the average competence duration between the two strains. As shown in the right plot of

**Figure S9**, in which the distribution of competence times of the SynEx strain has been rescaled such that it has the same average value as the native strain, but maintains its original coefficient of variation. In this case, the order of the sigmoidal is  $n=8.10\pm 0.60$ , very similar to the value corresponding to the original distribution. This result demonstrates that the slope of the sigmoid curve, and thus the sensitivity to extracellular DNA concentrations, is a function of the width of competence duration time distribution and not the mean.

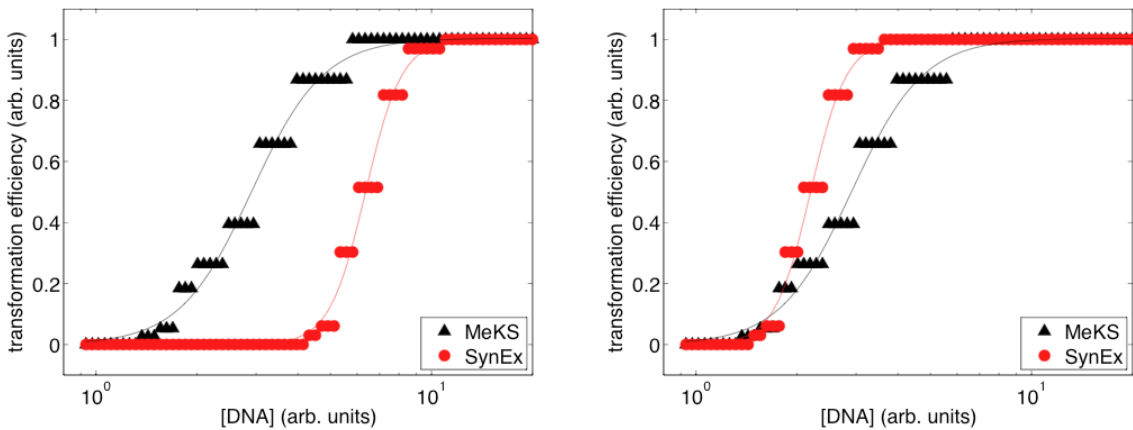


**Figure S9.** Transformation efficiency of the native and SynEx circuits for increasing amounts of exogenous DNA concentration, as computed from the experimentally measured distribution of competence durations. The solid lines are fits to sigmoidal functions, as a guide to the eye. Left: raw data where the competence time distributions have different averages. Right: the SynEx distribution is rescaled so that both native and SynEx have the same average, while each distribution maintains its coefficient of variation.

## S2. MATERIALS AND METHODS

### S2.1. Basic strain construction

The *Bacillus subtilis* strains used in this study are listed in Table S6. All strains are isogenic to wild-type *B. subtilis* PY79 strain. Strains were constructed using chromosomal integration vectors; pSac-Cm which integrates into the *sacA* locus, pGlt-Kan which is designed to integrate at the *gltA* locus (Middleton and Hofmeister, 2004). The plasmid pDR111 has an IPTG (Isopropyl  $\beta$ -D-1-thiogalactopyranoside)-inducible promoter (pHyperspank) which integrates into amyE gene (kind gifts of David Rudner, Harvard Medical School). The bifunctional cloning plasmid pHP13 carrying the replication function of the cryptic *B. Subtilis* plasmid pTA1060 (5 copies per genome) (Haima et al., 1987)

Isogenic <i>B. subtilis</i> PY79 strains	Genotype
P <sub>hyp</sub> -yfp	<i>amyE</i> :: P <sub>hyperspank</sub> -yfp (Sp <sup>R</sup> )
P <sub>comS</sub> -yfp ( $\beta$ S)	<i>amyE</i> :: pDL30-P <sub>comS</sub> -yfp (Sp <sup>R</sup> )
P <sub>comG-Kbox1</sub> -yfp	<i>amyE</i> :: P <sub>comG</sub> -cfp (Sp <sup>R</sup> ) <i>sacA</i> :: pSac-cm- P <sub>comG-Kbox1</sub> -yfp , P <sub>comG</sub> -cfp, (Cm <sup>R</sup> )
$\Delta$ comS	<i>sacA</i> :: pSac-cm-P <sub>comG</sub> -cfp (Cm <sup>R</sup> ) $\Delta$ <i>srfA</i> , <i>comS</i> :: <i>neo</i> (Neo <sup>R</sup> )
$\Delta$ comS-rescue	<i>amyE</i> :: P <sub>hyperspank</sub> - <i>comS</i> (Sp <sup>R</sup> ) <i>sacA</i> :: pSac-cm-P <sub>comG</sub> -cfp (Cm <sup>R</sup> ) $\Delta$ <i>srfA</i> , <i>comS</i> :: <i>neo</i> (Neo <sup>R</sup> )
SynEx	<i>amyE</i> :: P <sub>hyperspank</sub> - <i>comS</i> (Sp <sup>R</sup> ) <i>sacA</i> :: pSac-cm- P <sub>comG-Kbox1</sub> - <i>mecA</i> <sup>XP</sup> (Cm <sup>R</sup> ) $\Delta$ <i>srfA</i> , <i>comS</i> :: <i>neo</i> (Neo <sup>R</sup> ), P <sub>comG</sub> -cfp
SynExSlow	<i>amyE</i> :: P <sub>hyperspank</sub> - <i>comS</i> (Sp <sup>R</sup> ) <i>sacA</i> :: pSac-cm- P <sub>comG-Kbox1</sub> - <i>mecA</i> <sup>XP</sup> , P <sub>comG</sub> - <i>comS</i> :: (Cm <sup>R</sup> ) $\Delta$ <i>srfA</i> , <i>comS</i> :: <i>neo</i> (Neo <sup>R</sup> ), , P <sub>comG</sub> -cfp
WeakS	<i>amyE</i> ::pDL30- P <sub>comS</sub> - <i>comS</i> <sup>D29A</sup> (Sp <sup>R</sup> ) <i>sacA</i> :: pSac-cm - P <sub>comS</sub> - <i>comS</i> <sup>D29A</sup> (Cm <sup>R</sup> ) $\Delta$ <i>srfA</i> , <i>comS</i> :: <i>neo</i> (Neo <sup>R</sup> ), P <sub>comG</sub> -cfp
HighS	<i>amyE</i> ::pDL30- P <sub>comS</sub> -yfp, P <sub>comG</sub> -cfp (Sp <sup>R</sup> ) pHP13-P <sub>comS</sub> - <i>comS</i> (Cm <sup>R</sup> /Erm <sup>R</sup> ) <i>gltA</i> :: pGlt-Kan- P <sub>mecA</sub> - <i>mecA</i> (Kan <sup>R</sup> )

**Table S6.** Bacillus subtilis strain list.

## S2.2. Promoter definitions

P<sub>comG</sub>: chromosomal sequence 2559328 to 2559937 of the *comG* loci (minus-strand) was amplified from *B. subtilis* PY79 chromosomal DNA with reverse primer carrying a optimized ribosomal binding sequence (RBS) AAGGAGGAA. 609-base pair (bp) P<sub>comG</sub> region spans a RNA polymerase major Sigma factor (-49:+17 with respect to the transcription start site) binding site, and two cis-elements for the transcription factor, ComK at absolute chromosomal position 2559361 to 2559398 and 2559398 to 2559433, respectively.

P<sub>rpsD</sub>: chromosomal sequence 3034263 to 3034577 of the *ribosomal protein S4 (BS4)* loci (plus-strand) was Polymerase Chain Reaction (PCR) amplified from *B. subtilis* PY79 chromosomal DNA with reverse primer carrying a RBS. High level constitutive expression activity of the *rpsD* promoter has been reported previously (Jester et al., 2003).

P<sub>comS</sub>: chromosomal sequence 375859 to 376404 of the *srfAA-srfAB-comS-srfAC-srfAD* operon (plus-strand) was Polymerase Chain Reaction (PCR) amplified from *B. subtilis* PY79 chromosomal DNA with reverse primer carrying a RBS. 545-bp P<sub>comS</sub> region spans a RNA polymerase major Sigma factor -46:+17 with respect to the transcription start site) binding site, a PerR binding site (between a chromosomal position 376072 to 376122), a CodY binding site (between a chromosomal position 376197 to 376283, minus-stand) and two cis-elements for the transcription factor, ComA at absolute chromosomal position 376117 to 376154 and 376161 to 376198, respectively.

P<sub>mecA</sub>: *B. subtilis* PY79 chromosomal sequence 1228089 to 1223330 of the *mecA* loci (plus-strand) was assigned as the *mecA* promoter region with a RNA polymerase major Sigma factor (-48:+17 with respect to the transcription start site) binding site.

## S2.3. Construction of the SynEx strain

The Synthetic Excitable (SynEx) strain was constructed in three steps described below (Figure S10). All plasmids were transformed into *E. coli* DH5 $\alpha$  using standard methods. All *B. subtilis* promoters were PCR amplified from PY79 chromosomal DNA using Phusion DNA polymerase (NEB, USA). All transformations with cells of *B. subtilis* were carried out by a one-step transformation procedure (Jarmer et al., 2002). The genomic integrations of all constructs were verified by PCR and sequencing of corresponding antibiotic resistant transformants.

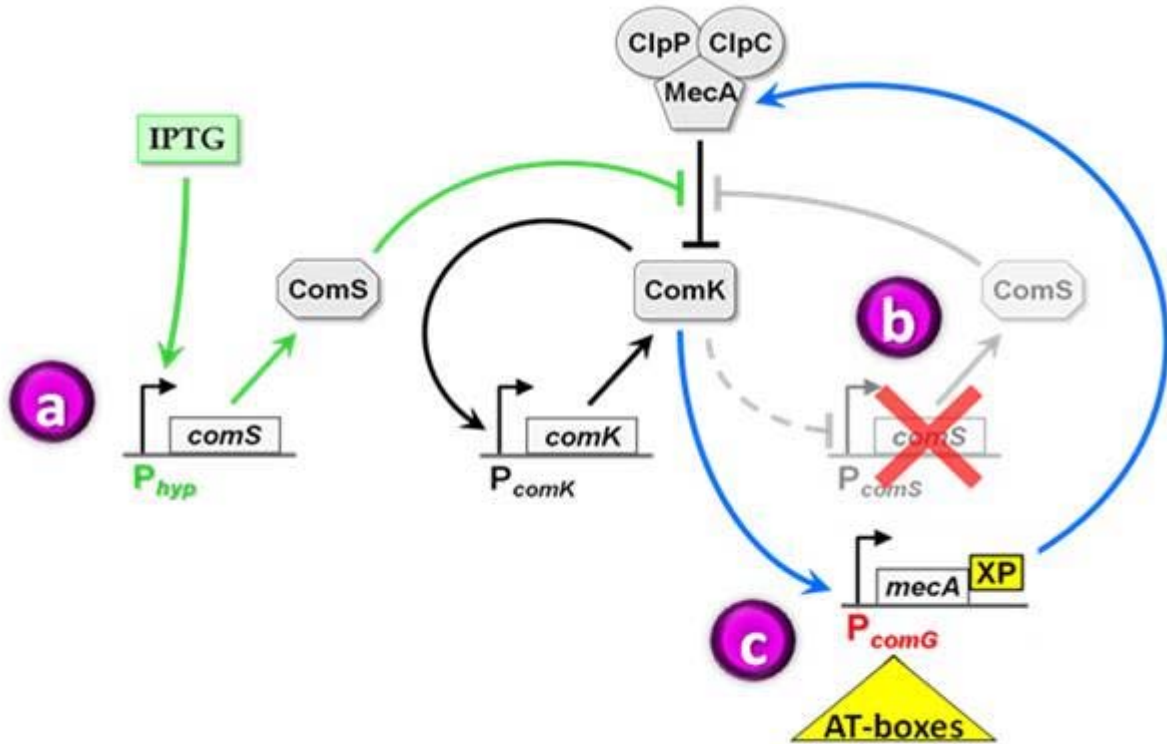


**Figure S10.** Schematic presentation of the Synthetic Excitable (SynEx) strain construction. (a) Introduction of an IPTG-inducible *comS* expression cassette. (b) Deletion of the *B. subtilis* endogenous *comS* gene resulted in removal of the native ComS-mediated indirect negative feedback loop (light gray loop). (c) Introduction of a synthetic negative feedback loop via  $P_{comG-Kbox1-mecA^{XP}}$  (blue loop). See text for details.

### S2.3.1 Introduction of an IPTG-inducible *comS* expression cassette into *B. subtilis* chromosomal DNA

pDR111-*comS* ( $P_{hyperspank-comS}$ ) construct (described in Süel G. *et al*, 2007(Süel et al., 2007)) was stably transformed into *B. subtilis amyE* locus.

### S2.3.2 Deletion of the *B. subtilis* endogenous *comS* gene

The 390431 to 390431 (5'-arm) and 390631 to 391247 (3'-arm) plus-stand regions of the *srfA* operon, on both sides of the *comS* coding sequence, were PCR amplified and cloned into per449 plasmid, carrying a neomycin (neo) resistance marker (kind gifts of Wade C. Winkler, UT Southwestern Medical Center). The coding sequence of cyan fluorescent protein (cfp) (obtained from pDH5 plasmid, University of Washington Yeast Resource Center) was PCR amplified, and was fused to wild-type (wt)  $P_{comG}$  promoter (described in section S2.2) using standard fusion PCR. Amplified competence-specific reporter cassette;  $P_{comG}$ -cfp was then cloned in between the 5'-and 3-arm, next to the neo gene. The resulting *comS* targeted deletion construct was integrated into the chromosome of *B. subtilis* by double cross-over ectopic integration.

### S2.3.3 Introduction of SynEx negative feedback loop via $P_{comG-Kbox1-mecA^{XP}}$ construct

The coding sequence of *mecA* including the native terminator was PCR amplified, and was fused to wild-type (wt)  $P_{comG}$  promoter (described in section S2.2.) using standard fusion PCR techniques. The amplified  $P_{comG-mecA}$  fragment was cloned into a pSacA-cm vector. To obtain a mutated AT-box1 in the *comG* promoter, the thymine (T) at position 2 in the T stretch of AT-box 1 was mutated into a guanine (G) by amplifying the  $P_{comG}$  promoter fragment with single-point mismatch primer from the pSacA-cm-  $P_{comG-mecA}$  construct. Finally, the *ssrA* mediated rapid degradation tag (AGKTNSFNQNVALAA) was introduced in between the *mecA* coding sequence and the native terminator sequence using standard fusion PCR technique. The final construct is named as pSacA-cm-  $P_{comG-Kbox1-mecA^{XP}}$ .

## S2.4. Optimization of the SynEx circuit

### S2.4.1 IPTG calibration of $P_{Hyperspank-ComS}$ , for appropriate competence frequency

Expression of ComS is necessary to permit the activation of the ComK positive feedback loop and thus competence (Maamar and Dubnau, 2005). Therefore, to compensate for *comS* deletion in the SynEx strain, we calibrated ComS expression driven by IPTG-inducible  $P_{hyperspank}$  promoter ( $P_{hyperspank-comS}$ ). The goal of the calibration was to obtain similar levels of ComS expression in SynEx cells compared to non-competent native cells with the difference that expression of ComS in SynEx cells would be constitutive and no longer be regulated by the competence circuit. Accordingly, we determined the dose response curve of  $P_{hyperspank-yfp}$  fluorescence as a function of IPTG concentrations in wild-type *B. subtilis* cells grown under standard movie conditions, described below. In conjunction we simultaneously measured the native expression from  $P_{comS}$  promoter using  $P_{comS-yfp}$  in wild-type non-competent cells. As show in Figure S11, this allowed us to approximately calibrate  $P_{hyperspank-yfp}$  activity in units of  $P_{comS-yfp}$  in non-competent native cells. Concurrently, a final concentration of 20  $\mu$ M IPTG in movie conditions resulted in a similar frequency of competence in SynEx cells compared to native. Introduction of IPTG had no effect on competence in native cells.

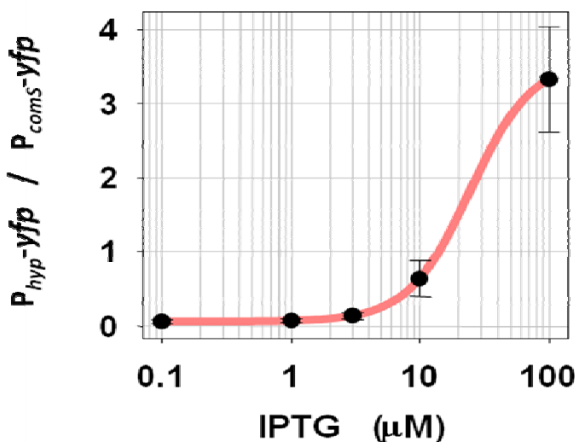


**Figure S11.** Dose response curve of  $P_{hyperspank-yfp}$  to IPTG. Shown are  $P_{hyperspank-yfp}$  levels as a function of log IPTG concentration. Fluorescence levels were measured at 7 and 20 hours of growth on IPTG pads as indicated alongside  $P_{comS-yfp}$  for calibration. 20  $\mu$ M IPTG induction was used to obtain a similar frequency of competence in SynEx cells compared to wild type. Error bars indicate standard error of the mean (S.E.M.)

### S2.4.2 Tuning the affinity of the $P_{comG}$ promoter ( $k_m$ )

In *B. subtilis* a consensus promoter binding sequence of two AAAA(N)<sub>5</sub>TTTT for ComK has been identified and termed K-box (Susanna et al., 2007). Promoters with this K-box motif play a central role in development of competence episodes. Two K-box motifs are typically separated by either 8, 18, or 31 base pairs. Susanna *et al.* have demonstrated that a single point mutation at the second T residue in the first AT-box (T to G replacement) resulted in a threefold reduction in transcription activation and DNA binding by ComK.

Mathematical modeling predicted that reduction in the affinity of the  $P_{comG}$  promoter for ComK may be required in order to obtaining competence events in SynEx cells (See section S1.2.2). To reduce this affinity, a single T to G mutation was introduced into first AT-box motif of  $P_{comG}$  in the pSacA-cm- $P_{comG}$ -*mecA* construct yielding  $P_{comG}$ -Kbox1 (as described in section S2.3.3). We then tested the effect of this point mutation on the expression dynamics of the  $P_{comG}$  promoter at the single-cell level by comparing the dynamics of the wild-type  $P_{comG}$  and AT-box1 mutated  $P_{comG}$ -Kbox1. Specifically, we constructed YFP expression cassettes with both promoters using standard fusion PCR technique, and cloned into pSacA-cm ectopic integration vector. Then each construct, pSacA-cm- $P_{comG}$ -Kbox1-*yfp* or pSacA-cm- $P_{comG}$ -*yfp* was integrated into the PY79  $P_{comG}$ -*cfp* strain. We then measured simultaneously YFP and CFP fluorescence in single cells under standard movie conditions. By directly comparing YFP fluorescence of either  $P_{comG}$ -Kbox1-*yfp* or  $P_{comG}$ -*yfp* versus  $P_{comG}$ -*cfp*, we were able to determine the effect of the AT-box1 mutation at the single-cell level (Figure S12).

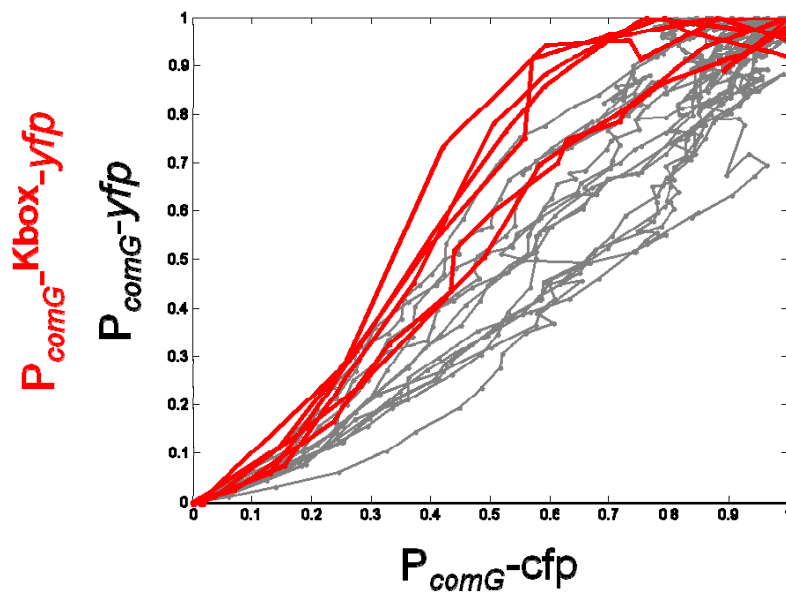


**Figure S12.** Quantitative time traces of PcomG-yfp (gray lines) or PcomG-Kbox1-yfp (red lines) simultaneously measured as functions of PcomG-cfp promoter activity in the same cell undergo competence.

### S2.4.3 Tuning MecA degradation

Expression of the adaptor protein *mecA* gene in *B. subtilis* has been reported to be approximately constant over time and in different growth media and conditions (Kong et al., 1993). To favor transiently elevated levels of MecA expressed from the  $P_{comG}$  promoter, we increased the degradation rate of MecA by introducing the well characterized *ssrA* gene mediated rapid degradation; AGKTNSFNQNALAA (Wiegert and Schumann, 2001) between the coding sequence of *mecA* and its native terminator sequence (Sierra N., 2008). Without this degradation tag, MecA expressed from  $P_{comG}$  would accumulate and persist in competent cells even after exit from competence.

### **S2.5. Construction of the WeakS strain**

An analysis of ComS by alanine-scanning mutation identified a ComS mutant D29A ( $ComS^{D29A}$ ) conferring approximately 50% of the wild type comS activity in  $P_{comG}$ -*lacZ* assay (Ogura et al., 1999). To increase the cellular ComS protein levels while maintaining the wild type ComS activity level and the same architecture as native *B. subtilis*, we constructed the WeakS strain which carries two copies of the  $ComS^{D29A}$  under native *comS* promoter ( $P_{comS}$ - $ComS^{D29A}$ ).  $P_{comS}$ - $ComS^{D29A}$  was fusion PCR amplified and cloned into both pSac-Cm and pDL30 integration plasmids. Then each construct was integrated into PY79 genome at *sacA* and *amyE* loci, respectively. Finally, deletion of the *B. subtilis* endogenous *comS* gene was achieved as described in section S2.3.2.

### **S2.6. Construction and analysis of the HighS strain**

As a secondary approach, to increase the cellular ComS protein level in a native cell, we have constructed the HighS strain. First we introduced a copy of the *comS* gene under its native promoter (see section S2.2) utilizing the low copy number plasmid pHP13 (5 copies per cell) than a second copy of the *mecA* gene under its native promoter (describe in section S2.2) was integrated into wild type PY79 background using pGlt-kan integration vector. (Figure S13).

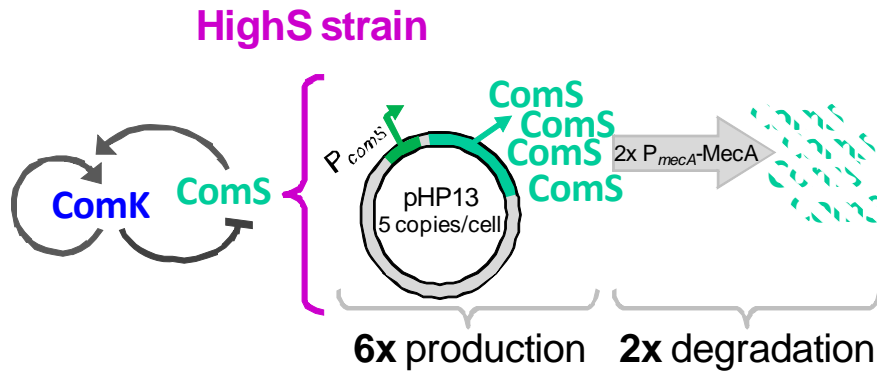


**Figure S13.** Schematic presentation of the HighS strain construction. See text for details

ComS, likewise comK, can binds to amino-terminal of MecA (Persuh et al., 1999), (Turgay et al., 1997). This competitive binding of ComS to MecA promotes the displacement of ComK from the degradation complex, and eventually leads to degradation of both ComS and MecA by ClpC protease, (Turgay et al., 1998) (Jenal and Hengge-Aronis, 2003), (Prepiak and Dubnau, 2007). Together, six-fold increase in ComS expression and two-fold increase in degradation were predicted to increase ComS molecule numbers subsequently produce a lower variability in competence duration as compared to native competence event (Figure S14).

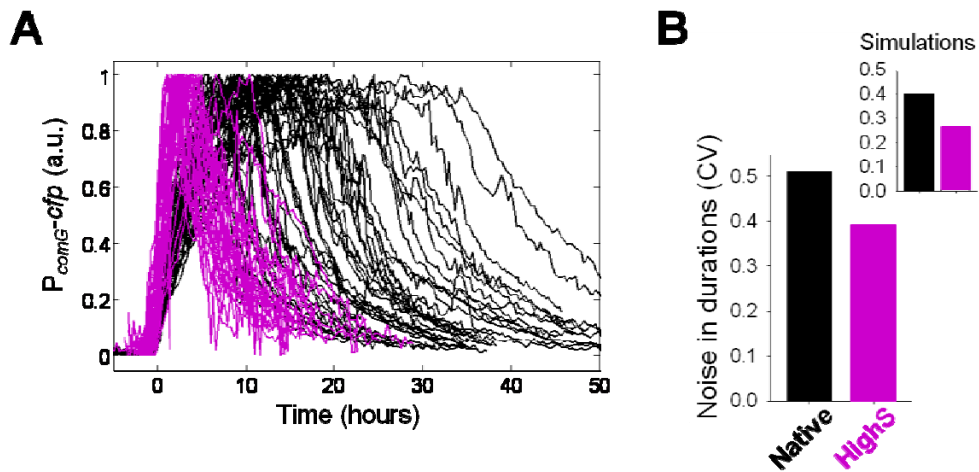


**Figure S14.** (A) Fluorescence time traces, normalized by their maximum value, from  $P_{comG-cfp}$  in the HighS strain (purple, n=38) and the wild type (black, n=91). Traces have been aligned with respect to time of initiation of  $P_{comG}$  expression. (B) Time-lapse microscopy measurements of competence duration in HighS strain reveal that, as suggested by simulations, noise in the competence duration reduced by 24% as compared to wild type.

## S2.7. Construction of the SynExSlow strain

To increase the duration of competence events generated by the SynEx circuit, we constructed the SynExSlow strain. In the SynExSlow strain, competence durations are prolonged by reducing the strength of the MecA mediated negative feedback loop of the SynEx circuit that controls the degradation of ComK (Figure S15). Specifically, we utilized the competition between ComK and ComS for binding to MecA. A single copy of fusion PCR amplified PcomG-comS fragment was introduced into the pSacA-cm- PcomG-Kbox1-mecAXP construct. Exclusive expression of this additional copy of comS from the tightly controlled ComK-specific comG promoter (Hamoen et al., 1998; Susanna et al., 2004) during competence competes directly with ComK for binding, to MecA. Therefore, ComS acts by direct competition to reduce degradation of ComK by MecA exclusively during competence (Prepiak and Dubnau, 2007). As expected and shown in table S7, the frequency of initiation and exit from competence in the SynExSlow strain is unaltered from SynEx.

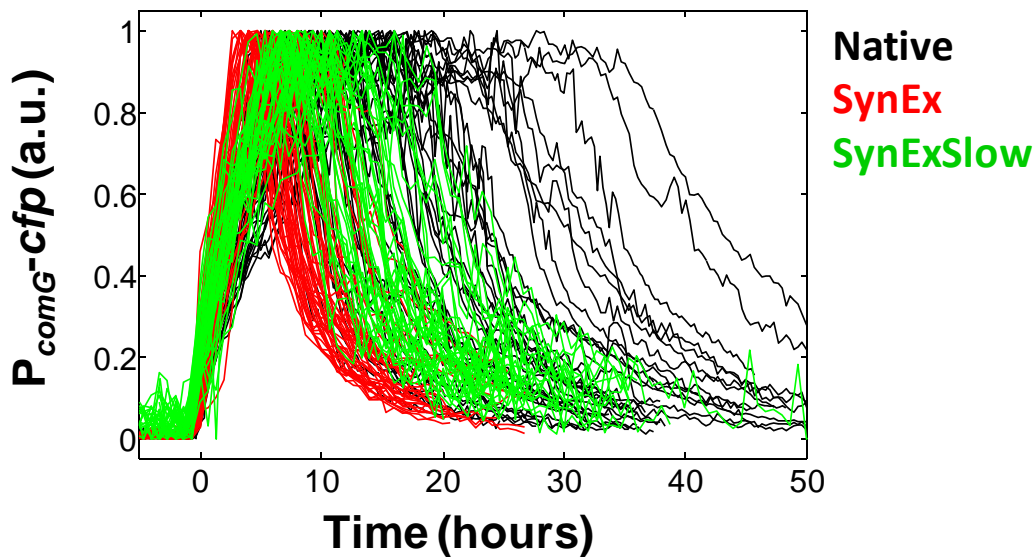


**Figure S15.** Fluorescence time traces, normalized by their maximum value, from  $P_{comG-cfp}$  in the SynEx, SynExSlow strains or the wild type. Traces have been aligned with respect to time of initiation of  $P_{comG}$  expression.

## S2.8. Strain Statistics

Isogenic <i>B. subtilis</i> PY79 strains	$P_{\text{init}}$ (%)	$P_{\text{exit}}$ (%)	Mean duration of competence episode (hours)
Wild type	$3.6 \pm 0.7$	61	17.4
$\Delta\text{comS}$ -rescue	$7.7 \pm 1.5$	$8 \pm 1.1$	NA
SynEx	$3.9 \pm 0.5$	$80 \pm 1.1$	7.8
SynExSlow	$3.1 \pm 0.3$	$81 \pm 0.8$	16.5
WeakS	$0.5 \pm 0.12$	$64 \pm 10.8$	9.5
HighS	$1.5 \pm 0.05$	$96 \pm 1.8$	7.5

**Table S7.** Summary table for strain statistics : The probability of competence initiation ( $P_{\text{init}}$ ) and that of competence exit ( $P_{\text{exit}}$ ) in movies of strains was determined as follows (minimum 5 independent experiments): Under conditions that allow initiation of competence (see section S2.10),  $P_{\text{init}}$  was defined as the number of competence initiation events divided by the total number of cell division events within this time frame (200 min), and the  $P_{\text{exit}}$  value was defined as the fraction of competent cells that successfully leave the competent state. NA; not applicable –cells stuck in competence which eventually led to death of cells.

## S2.9. Transformation of *B. subtilis* strains

First we constructed an integrative expression plasmid pDP150- $P_{\text{rpsD}}$ -*yfp* to perform the transformation assays and determine their efficiency. The Spectinomycin resistance gene was excised from the pDP150 chromosomal integration vector (kind gift of Richard M. Losick, Harvard University), by double digestion with SmaI and MscI endonucleases. The linearized vector was then self-ligated. The coding sequence of yellow fluorescent protein (*yfp*) was PCR amplified, and fused to  $P_{\text{rpsD}}$  promoter (described in section S2.2) using standard fusion PCR. This constitutive *yfp* expression cassette  $P_{\text{rpsD}}$ -*yfp* was then introduced into the pDP150 vector, to obtain pDP151- $P_{\text{rpsD}}$ -*yfp* integrative expression plasmid.

SynEx, SynExSlow, WeakS and parental PY79 (native) strains were streaked on a Luria-Bertani (LB) broth agar plate and incubated overnight at 37°C with appropriate antibiotics. Cells from a single colony were inoculated in 10 ml of glucose minimal medium as described in Jarmer *et al.* with glutamate as the sole nitrogen source. The culture was grown at 37°C in a 25-ml flask with good aeration to an optical density ( $\text{OD}_{600}$ ) of  $\sim 0.8$ . 1 ml of this culture cells was incubated with the integrative expression plasmid pDP151- $P_{\text{rpsD}}$ -*yfp* that confers erythromycin (Erm) resistance, and constitutive *yfp* expression upon integration into the *thrC* locus at 37°C for 40 min. SynEx and SynExSlow cells were supplemented with 20  $\mu\text{M}$  IPGT during this 40 min incubation in accordance with Section S2.4.1. Following the 45 min growth in 2XYT media, cells were plated on Erm-LB agar plates and incubated overnight at 37°C. YFP positive individual colonies were counted under fluorescence Olympus SZX7 stereo microscope system to calculate the transformation efficiency. Randomly selected transformants were also independently confirmed for correct genomic integration with conventional PCR.

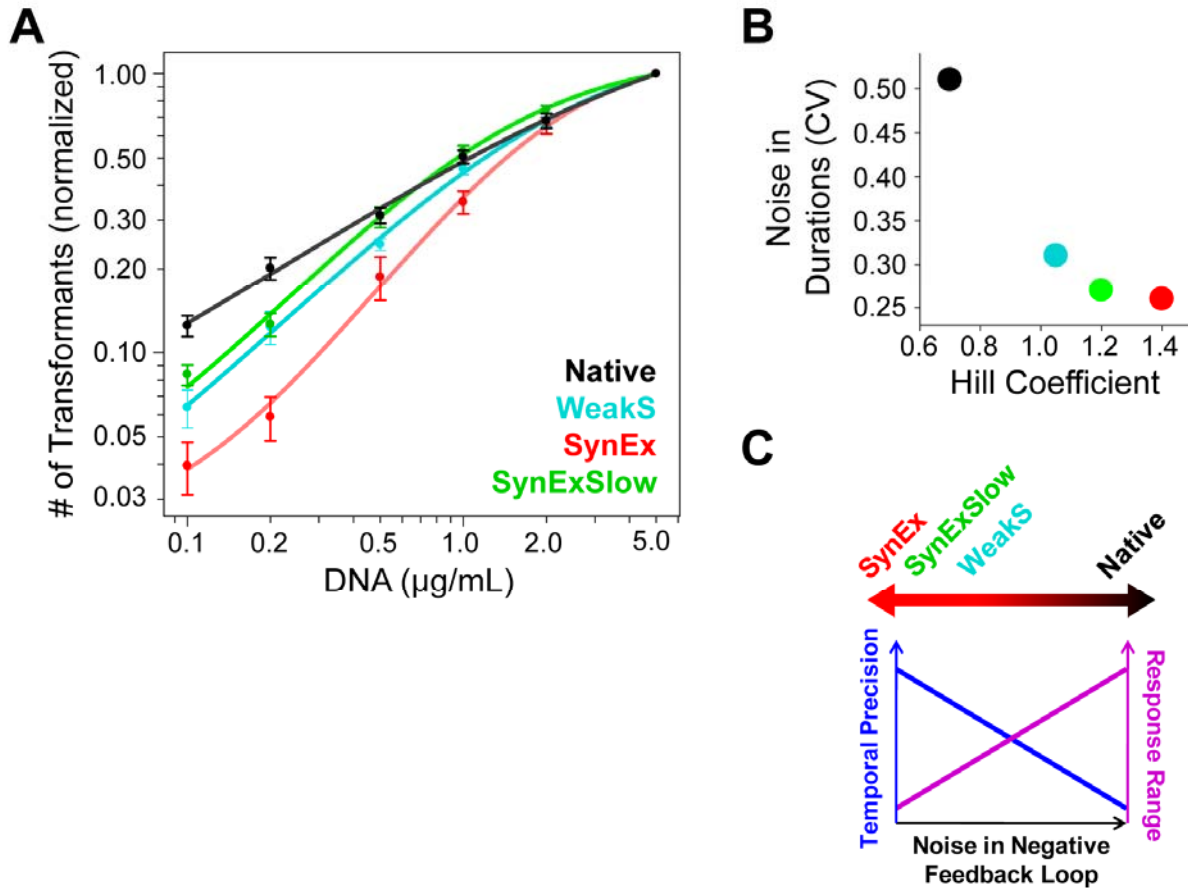


**Figure S16.** Noise in competence durations times in native cells increases robustness of competence physiology under varying extracellular DNA concentrations. **(A)**, doubly logarithmic plot of the number of transformants normalized to the same maximum value, as a function of DNA concentrations. Normalization permits direct visual comparison of relative change in transformation efficiency as a function of extracellular DNA concentrations among the strains. Data points depict mean and S.E.M. of a minimum of 7 independent experiments with a total of 83,000 colonies counted for native (black), WeakS (cyan), SynEx (red) and SynExSlow (green) strains. To permit direct comparison, all strains were transformed with the same plasmid. Solid lines represent fits of the data to a standard sigmoidal Hill function. The Hill coefficients of the respective dose response curves are 0.7 for the native, 1.1 for WeakS, 1.2 for SynExSlow and 1.4 for the SynEx circuits. **(B)**, correlation plot of noise (coefficient of variance) in competence durations versus Hill coefficient obtained from transformation response curves for native (black), WeakS (cyan), SynEx (red) and SynExSlow (green) strains. Higher noise in competence duration times correlates with lower Hill coefficient. **(C)**, cartoon depicting the tradeoff between temporal precision of single cell dynamics and response range at the population level that appears to be regulated by noise in the negative feedback loop regulator.

## S2.10. Imaging and growth conditions

*B. subtilis* cells were grown in LB at 37°C. Antibiotics for selection were added to the following final concentrations: 5 μg/ml chloramphenicol, 5 μg/ml neomycin, 10 μg/ml spectinomycin and erythromycin, 5 μg/ml. When necessary, the cultures were adjusted to the final IPTG concentrations of 20 μM. Unless stated otherwise, all growth and imaging conditions were performed as described previously (Süel et al., 2006).

### S2.10.1 Preparation for microscopy

Conditioned Media (CM) was prepared by growing of a single colony of the wild-type *B. subtilis* (PY79) in 2m of fresh LB for 6 hours (hrs), then all of the cells were diluted in 23 ml fresh LB and were grown for additional 18 hrs at 37°C. Subsequently, cells were pelleted at 5000 rpm for 10 min, and were grown in resuspension medium (RM) for 30 hrs. After the final 30 hr incubation, cells were removed by centrifugation (at 5000 rpm for 10 min), and the supernatants were sterilized by filtration through 0.2- $\mu$ m-pore-size filters. Conditioned medium was stored at -80°C.

Cells were grown at 37C in LB to an O.D. of 1.8 and resuspended in 0.5 volume of RM(Sterlini and Mandelstam, 1969) supplemented with 20  $\mu$ M IPTG. After 1.5 hour incubation at 37°C, cells were diluted 10-fold in RM and applied onto a 1.5% low melting agarose pad made with RM supplemented with 20  $\mu$ M IPTG and 2% CM. This protocol is optimized for time-lapse microscopy. RM reduces the growth rate of microcolonies on agarose and leads to sporulation, while 2% CM was used as growth supplement.

### 2.10.2 Image analysis

Image analysis was performed as described previously in Süel *et al*, 2006 (Süel et al., 2006).

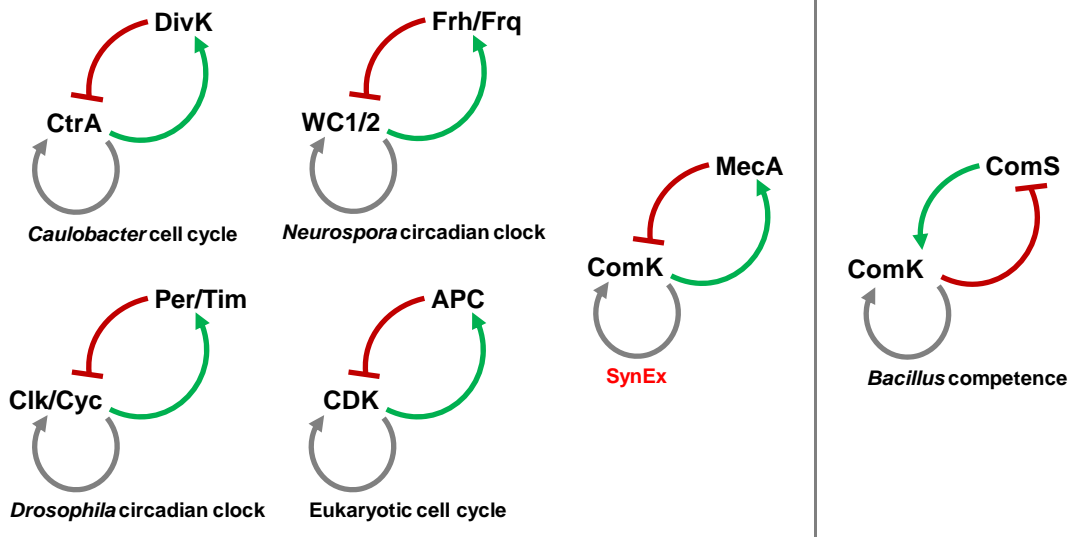


**Figure S17.** Comparison of *B. subtilis* native and SynEx competence circuits to examples of genetic oscillators from diverse organisms. Note that genetic oscillators share the negative feedback loop polarity of the SynEx and not that of the native competence circuit.

## Supplemental References

- Gillespie, D.T. (1976). A general method for numerically simulating the stochastic time evolution of coupled chemical reactions *Journal of Computational Physics* *22*, 403-434.
- Gillespie, D.T. (1977). Exact Stochastic Simulation of Coupled Chemical Reactio. *The Journal of Physical Chemistry* *81*, 2340-2361.
- Haima, P., Bron, S., and Venema, G. (1987). The effect of restriction on shotgun cloning and plasmid stability in *Bacillus subtilis* Marburg. *Mol Gen Genet* *209*, 335-342.
- Hamoen, L.W., Van Werkhoven, A.F., Bijlsma, J.J., Dubnau, D., and Venema, G. (1998). The competence transcription factor of *Bacillus subtilis* recognizes short A/T-rich sequences arranged in a unique, flexible pattern along the DNA helix. *Genes Dev* *12*, 1539-1550.
- Jarmer, H., Berka, R., Knudsen, S., and Saxild, H.H. (2002). Transcriptome analysis documents induced competence of *Bacillus subtilis* during nitrogen limiting conditions. *FEMS Microbiol Lett* *206*, 197-200.
- Jenal, U., and Hengge-Aronis, R. (2003). Regulation by proteolysis in bacterial cells. *Curr Opin Microbiol* *6*, 163-172.
- Jester, B.C., Levengood, J.D., Roy, H., Ibba, M., and Devine, K.M. (2003). Nonorthologous replacement of lysyl-tRNA synthetase prevents addition of lysine analogues to the genetic code. *Proc Natl Acad Sci U S A* *100*, 14351-14356.
- Kong, L., Siranosian, K.J., Grossman, A.D., and Dubnau, D. (1993). Sequence and properties of *mecA*, a negative regulator of genetic competence in *Bacillus subtilis*. *Mol Microbiol* *9*, 365-373.
- Maamar, H., and Dubnau, D. (2005). Bistability in the *Bacillus subtilis* K-state (competence) system requires a positive feedback loop. *Mol Microbiol* *56*, 615-624.
- Middleton, R., and Hofmeister, A. (2004). New shuttle vectors for ectopic insertion of genes into *Bacillus subtilis*. *Plasmid* *51*, 238-245.
- Ogura, M., Liu, L., Lacelle, M., Nakano, M.M., and Zuber, P. (1999). Mutational analysis of ComS: evidence for the interaction of ComS and MecA in the regulation of competence development in *Bacillus subtilis*. *Mol Microbiol* *32*, 799-812.
- Ozbudak, E.M., Thattai, M., Kurtser, I., Grossman, A.D., and van Oudenaarden, A. (2002). Regulation of noise in the expression of a single gene. *Nat Genet* *31*, 69-73.
- Persuh, M., Turgay, K., Mandic-Mulec, I., and Dubnau, D. (1999). The N- and C-terminal domains of MecA recognize different partners in the competence molecular switch. *Mol Microbiol* *33*, 886-894.
- Prepiak, P., and Dubnau, D. (2007). A peptide signal for adapter protein-mediated degradation by the AAA+ protease ClpCP. *Mol Cell* *26*, 639-647.
- Sierro N., M.Y., de Hoon M.J.L. and Nakai K. (2008). DBTBS: a database of transcriptional regulation in *Bacillus subtilis* containing upstream intergenic conservation information (*Nucleic Acids Research*, 2008, Vol. 36, Database issue D93-D96).

- Smits, W.K., Eschevins, C.C., Susanna, K.A., Bron, S., Kuipers, O.P., and Hamoen, L.W. (2005). Stripping Bacillus: ComK auto-stimulation is responsible for the bistable response in competence development. *Mol Microbiol* 56, 604-614.
- Sterlini, J.M., and Mandelstam, J. (1969). Commitment to sporulation in *Bacillus subtilis* and its relationship to development of actinomycin resistance. *Biochem J* 113, 29-37.
- Süel, G.M., Garcia-Ojalvo, J., Liberman, L.M., and Elowitz, M.B. (2006). An excitable gene regulatory circuit induces transient cellular differentiation. *Nature* 440, 545-550.
- Süel, G.M., Kulkarni, R.P., Dworkin, J., Garcia-Ojalvo, J., and Elowitz, M.B. (2007). Tunability and noise dependence in differentiation dynamics. *Science* 315, 1716-1719.
- Susanna, K.A., Mironczuk, A.M., Smits, W.K., Hamoen, L.W., and Kuipers, O.P. (2007). A single, specific thymine mutation in the ComK-binding site severely decreases binding and transcription activation by the competence transcription factor ComK of *Bacillus subtilis*. *J Bacteriol* 189, 4718-4728.
- Susanna, K.A., van der Werff, A.F., den Hengst, C.D., Calles, B., Salas, M., Venema, G., Hamoen, L.W., and Kuipers, O.P. (2004). Mechanism of transcription activation at the comG promoter by the competence transcription factor ComK of *Bacillus subtilis*. *J Bacteriol* 186, 1120-1128.
- Turgay, K., Hahn, J., Burghoorn, J., and Dubnau, D. (1998). Competence in *Bacillus subtilis* is controlled by regulated proteolysis of a transcription factor. *EMBO J* 17, 6730-6738.
- Turgay, K., Hamoen, L.W., Venema, G., and Dubnau, D. (1997). Biochemical characterization of a molecular switch involving the heat shock protein ClpC, which controls the activity of ComK, the competence transcription factor of *Bacillus subtilis*. *Genes Dev* 11, 119-128.
- Wiegert, T., and Schumann, W. (2001). SsrA-mediated tagging in *Bacillus subtilis*. *J Bacteriol* 183, 3885-3889.